Journal of Power Sources 195 (2010) 4400–4405

Contents lists available at ScienceDirect

Journal of Power Sources

journal homepage: www.elsevier.com/locate/jpowsour

A porous spherical aggregation of $Li_4Mn_5O_{12}$ nanorods and its electrochemical performance

Yan Zhao, Qiongyu Lai*, Yanjing Hao, Hongmei Zeng, Hongyan Chu, Zhien Lin

College of Chemistry, Sichuan University, Chengdu 610064, PR China

ARTICLE INFO

Article history:
Received 2 October 2009
Received in revised form 26 January 2010
Accepted 28 January 2010
Available online 4 February 2010

Keywords:
$(NH_4)_2S_2O_8$
$Li_4Mn_5O_{12}$
Porous material
Spherical aggregation
Capacitance performance

ABSTRACT

A porous spherical aggregation of $Li_4Mn_5O_{12}$ nanorods with the particle size of 3 μm is prepared by oxidizing $LiMn_2O_4$ powder with $(NH_4)_2S_2O_8$ under hydrothermal conditions. The result displays that concentration of $(NH_4)_2S_2O_8$ plays a key role in forming the porous spherical aggregation and the optimal concentration of oxidant is found to be 1.5 mol L^{-1}. The mechanism for the formation of the porous spherical aggregation is proposed. The electrochemical capacitance performance is tested by cyclic voltammetry, electrochemical impedance spectroscopy and galvanostatic charge/discharge. The porous spherical aggregation exhibits a good electrochemical performance. It could deliver 375 F g^{-1} within potential range 0–1.4 V at a scan rate of 5 mV s^{-1} in 1 mol L^{-1} Li_2SO_4 and the value is cut down to less than 0.024 F g^{-1} per cycling period in 1000 cycles.

Introduction

One-dimensional (1D) nanostructure materials, such as nanotubes [1,2], nanowires [3,4], nanorods [5,6], nanoneedles [7] and nanochains [8], have been extensively studied due to their excellent physical and chemical properties and potential applications in electronics, photonics, and magnetic materials [9,10]. Up to now, transition metal oxides, for instance ZnO [11], MnO_2 [12], etc. have received considerable investigation among all of 1D nanostructure materials. Over the past decades, 1D nanostructure lithium ion battery materials are of particular interest because these materials exhibit excellent electrochemical performance, including higher discharge specific capacitance, longer cycling life and wider potential window. Recently, lithium manganese oxides, especially those with spinel structure type, have attracted considerable attention due to their low toxicity, low cost and environmentally friendliness, which are the most promising candidates to replace $LiCoO_2$ electrode materials [13,14].

Despite the extensive research on 1D $LiMn_2O_4$ nanostructure [15,16], little is known about $Li_4Mn_5O_{12}$ [13]. It is well-known that one of the key points in the synthesis of inorganic nanomaterial is to control its structure, size and shape because its physical/chemical properties are intimately correlated with these parameters [17]. Our previous study demonstrates that $Li_4Mn_5O_{12}$ nanoparticles were prepared by sol–gel method and these materials showed good electrochemical behavior [18,19]. To further improve the electrochemical performance of this material, a new synthetic approach has been developed to synthesize a porous spherical aggregation of $Li_4Mn_5O_{12}$ nanorods by oxidizing $LiMn_2O_4$ powder with $(NH_4)_2S_2O_8$ under low temperature hydrothermal conditions. Compared with conventional $Li_4Mn_5O_{12}$ nanoparticles, this porous spherical aggregation possesses several advantages. For example, it has larger surface area and much more electrochemistry interface reaction sites, resulting in higher discharge specific capacitance and excellent electrochemical performance. Furthermore, the porous spherical aggregation will be in favor of electrolyte dipping and electrode slice coating. In this method, the oxidant $(NH_4)_2S_2O_8$ played an important role in the formation of porous spherical aggregation, which has not been reported in the literatures. To the best of our knowledge, the mechanism related to the morphology formation of $Li_4Mn_5O_{12}$ was proposed and discussed for the first time.

Experimental

Preparation

The pristine $LiMn_2O_4$ was prepared according to the method described in the literature [20]. The obtained $LiMn_2O_4$ powder was dispersed in $(NH_4)_2S_2O_8$ solutions with different concentrations in a 50 mL Teflon-lined stainless-steel autoclave. The autoclave was heated at 65 °C for 24 h and then cooled to room temperature in air. The resulting $Li_4Mn_5O_{12}$ powders were washed repeatedly and then dried.

* Corresponding author. Tel.: +86 28 85416969; fax: +86 28 85416969.
E-mail address: laiqy5@hotmail.com (Q. Lai).

0378-7753/$ – see front matter © 2010 Elsevier B.V. All rights reserved.
doi:10.1016/j.jpowsour.2010.01.072

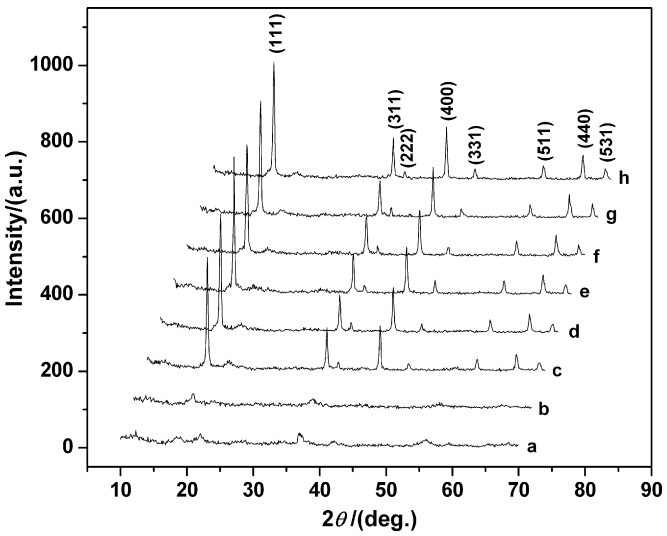

Fig. 1. XRD patterns of the $Li_4Mn_5O_{12}$ powders with different concentration of $(NH_4)_2S_2O_8$ solutions. (a) 0.1 mol L^{-1}, (b) 0.3 mol L^{-1}, (c) 0.5 mol L^{-1}, (d) 0.7 mol L^{-1}, (e) 1.0 mol L^{-1}, (f) 1.5 mol L^{-1}, (g) 2.0 mol L^{-1} and (h) 2.5 mol L^{-1}.

Characterization

Powder X-ray diffraction (XRD) data were collected on a D/MAX-rA diffractometer with Cu Kα radiation (λ = 0.15418 nm) operated at 40 kV and 100 mA. Scanning electron microscopy (SEM) was taken on a Philips Inspect F electron microscope at an accelerating voltage of 10 kV. The sample's surfaces were dried and sputter coated with gold prior to examination.

Electrode preparation and electrochemical performance test

The cathode was prepared by mixing 70 wt% of the active material ($Li_4Mn_5O_{12}$) with 25 wt% acetylene black (AB) and 5 wt% polyvinylidene fluoride (PVDF), using *N*-methyl-2-pyrrolidine (NMP) as solvent. After the mixture was blended sufficiently, the obtained slurry was dried in an infrared light oven for 5 h, and then pressed onto a stainless-steel grid. The anode was prepared by the same method mentioned above and it consisted of 65 wt% activated carbon (AC), 29 wt% AB and 6 wt% PVDF. The electrolyte for the test was 1 mol L^{-1} Li_2SO_4.

Cyclic voltammetry (CV) measurements were performed by using a three-electrode system, in which $Li_4Mn_5O_{12}$ were used as the working electrode, platinum as the counter electrode, and saturated calomel electrode (SCE) as the reference electrode. The measurement was carried out on a Tianjin Lanlike Electrochemi-

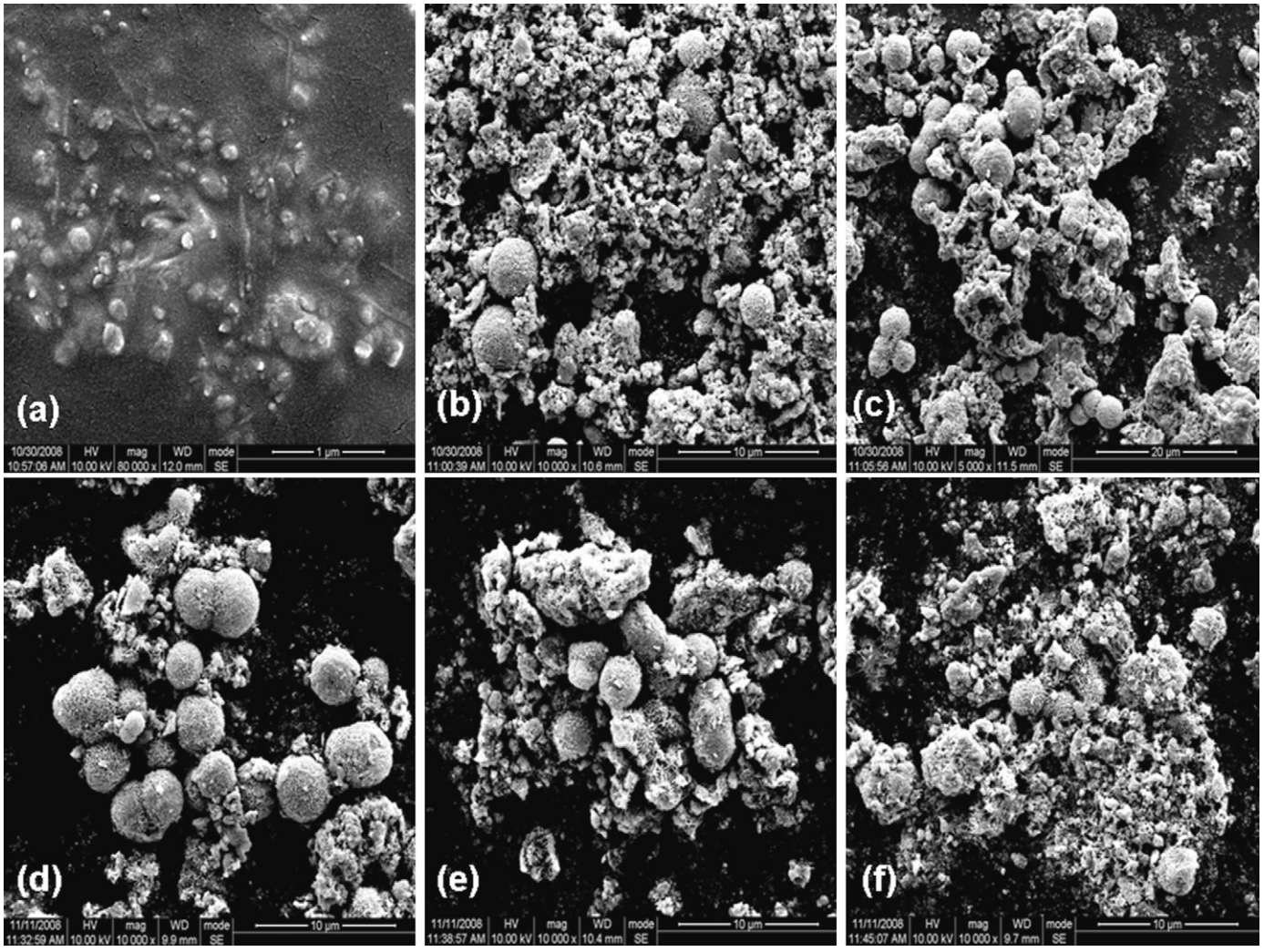

Fig. 2. SEM micrographs of the $Li_4Mn_5O_{12}$ treated by different concentration of $(NH_4)_2S_2O_8$ solutions. (a) 0.5 mol L^{-1}, (b) 0.7 mol L^{-1}, (c) 1.0 mol L^{-1}, (d) 1.5 mol L^{-1}, (e) 2.0 mol L^{-1} and (f) 2.5 mol L^{-1}.

cal Workstation (model LK2005) with the electrochemical interface controlled by computer.

Electrochemical impedance spectroscopy (EIS) measurements were carried out at frequencies from 10 kHz to 0.01 Hz by using an Autolab Electrochemical Workstation, which consists of a three-electrode system with $Li_4Mn_5O_{12}$ working electrode, platinum counter electrode and SCE reference electrode. The electrochemical interface and frequency response analyzer were controlled by a computer.

All the charge/discharge tests were performed by using Neware Cell Program Control Test System with current density of 100 mA g^{-1} in the range of 0–1.4 V at room temperature, which contains a two-electrode system.

Results and discussion

XRD analysis

Fig. 1 shows the XRD patterns of $Li_4Mn_5O_{12}$ with different concentrations of $(NH_4)_2S_2O_8$ treatment. When the concentration of $(NH_4)_2S_2O_8$ is lower than 0.5 mol L^{-1}, no $Li_4Mn_5O_{12}$ phase could be prepared under hydrothermal conditions, indicating the pristine $LiMn_2O_4$ could not be oxidized to $Li_4Mn_5O_{12}$ in this concentration. When the concentration of $(NH_4)_2S_2O_8$ is equal to or higher than 0.5 mol L^{-1}, it can be observed that the diffraction peak of the obtained products matched quite well with the typical fingerprint [21]. All the diffraction peaks can be indexed as a face-centered cubic spinel structure with a space group $Fd\bar{3}m$.

SEM analysis

The effect of different concentrations of $(NH_4)_2S_2O_8$ vs. sample morphology can be observed from SEM images in Fig. 2. As shown in Fig. 2a–c, little porous spherical aggregation could be observed and most products remain as nanorods, which are growing and reuniting to form aggregation when the concentration of $(NH_4)_2S_2O_8$ is lower than 1.5 mol L^{-1}. Under such a concentration, there is not enough SO_4^{2-}, which is the reduction product of $(NH_4)_2S_2O_8$, to induce nanorods to spontaneously aggregate into spheres. When the concentration of $(NH_4)_2S_2O_8$ is up to 1.5 mol L^{-1}, a great deal of porous spherical aggregation appears, as shown in Fig. 2d.

SEM image of $Li_4Mn_5O_{12}$ aggregation treated by 1.5 mol L^{-1} $(NH_4)_2S_2O_8$ is shown in Fig. 3a. The aggregation has a smooth surface and clear contour with the particle size of 3 μm. Careful analysis of the aggregation reveals that it is formed by a number of nanorods intertwisting and interweaving together.

Under suitable concentration of $(NH_4)_2S_2O_8$, it is easy for nanorods to assemble with each other to form aggregation due to the proper SO_4^{2-} concentration is provided. But with the continuous increase of $(NH_4)_2S_2O_8$ concentration until 2.0 and 2.5 mol L^{-1}, respectively, the number of porous spherical aggregation decreases. As can be seen in Fig. 2e and f, the aggregation disassembles to turn into nanorods, suggesting that higher concentrations are not favor for the formation of porous spherical aggregation.

Therefore, a conclusion is drawn that the concentration of $(NH_4)_2S_2O_8$ plays a vital role in the formation of the porous spherical aggregation of $Li_4Mn_5O_{12}$ nanorods. The higher or lower concentration goes against aggregation, herein a proper concentration, namely 1.5 mol L^{-1}, is needed.

Proposed mechanism for the formation of porous spherical aggregation

Fig. 3b shows the schematic representation for the formation of $Li_4Mn_5O_{12}$ porous spherical aggregation. First, $Li_4Mn_5O_{12}$ par-

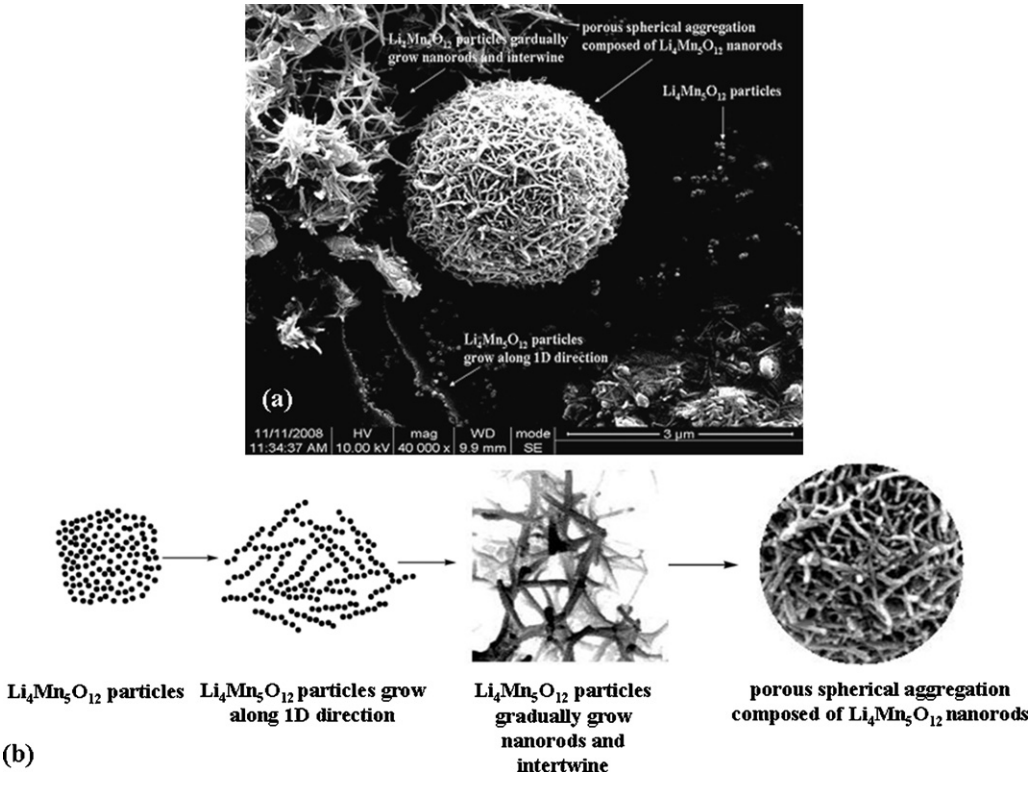

Fig. 3. (a) SEM micrograph of the porous spherical nanorods aggregation $Li_4Mn_5O_{12}$ with 1.5 mol L^{-1} of $(NH_4)_2S_2O_8$ treatment. (b) The schematic representation of the formation of porous spherical aggregation.

ticles are formed under hydrothermal conditions. Meanwhile, the self-assembly of adjacent particles make them to share a common crystallographic orientation [22,11], and the self-assembly of these particles from nanodots to nanorods can reduce overall energy. Thus, the particles grow along 1D direction to form nanorods which intertwist and interweave together due to the chemadsorption between SO_4^{2-} and nanorod surface.

In the synthetic system, there are electrostatic interaction between SO_4^{2-} anions and Mn^{4+} cations on $Li_4Mn_5O_{12}$ surface, coordinating bond of O atoms in SO_4^{2-} with Mn^{4+} ions and hydrogen bond of O atoms in SO_4^{2-} with H atoms of H_2O molecular on the nanorod surface; all might contribute to the chemadsorption. Such a process is somewhat similar to that in a previous report by Xu et al. [23]. When the concentration of $(NH_4)_2S_2O_8$ is lower than 1.5 mol L^{-1}, little porous spherical aggregation can be observed due to less SO_4^{2-} available in the system. When the concentration of $(NH_4)_2S_2O_8$ is up to 1.5 mol L^{-1}, the coordination bond between SO_4^{2-} and Mn^{4+} ions on the nanorod surface reaches the highest, hence the amount of aggregation increases. When the concentration of $(NH_4)_2S_2O_8$ is larger than 1.5 mol L^{-1}, there are much more dissociative SO_4^{2-} in the solution. When there are more SO_4^{2-} ions on the surface, the repelling force between SO_4^{2-} and SO_4^{2-} can result in the aggregation loosen and has a disintegration trend.

Electrochemical performance

CV analysis

Fig. 4 shows the cyclic voltammograms of $Li_4Mn_5O_{12}$ with different concentration of $(NH_4)_2S_2O_8$ treatment in 1 mol L^{-1} Li_2SO_4. It is clearly showed that the sample treated at 1.5 mol L^{-1} $(NH_4)_2S_2O_8$ exhibits the highest capacitance. The phenomenon can be considered that the more the porous spherical aggregation is, the more easily the sample contacts electrolyte, leading that $Li_4Mn_5O_{12}$ displays a good performance.

Fig. 5 shows the cyclic voltammograms of $Li_4Mn_5O_{12}$ with 1.5 mol L^{-1} $(NH_4)_2S_2O_8$ treatment in 1 mol L^{-1} Li_2SO_4 at different scan rates in the potential range from 0 to 1.4 V. From the results of CV, two pairs of redox peaks located at 0.4 and 0.8 V vs. SCE and at 0.6 and 1.0 V vs. SCE are observed for $Li_4Mn_5O_{12}$ at a scan rate of 2 mV s^{-1}. The single electrode discharge specific capacitance can be estimated from the voltammetric charge surrounded by the CV

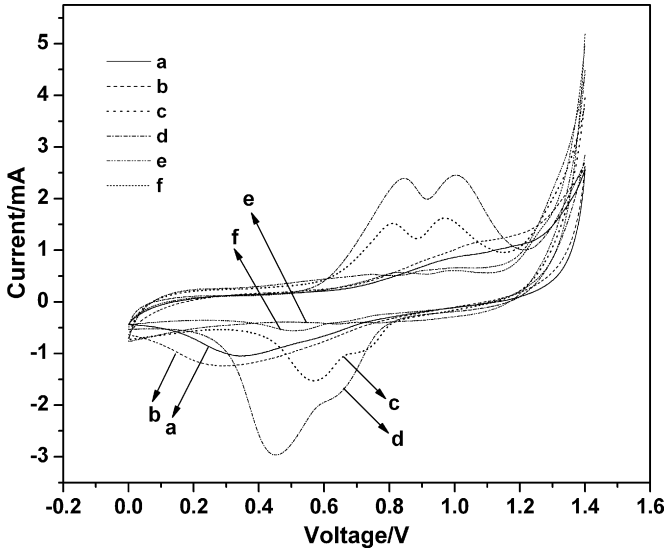

Fig. 4. CV curves of the $Li_4Mn_5O_{12}$ electrode with different concentration of $(NH_4)_2S_2O_8$ treatment at 5 mV s^{-1} scan rates in 1 mol L^{-1} Li_2SO_4. (a) 0.5 mol L^{-1}, (b) 0.7 mol L^{-1}, (c) 1.0 mol L^{-1}, (d) 1.5 mol L^{-1}, (e) 2.0 mol L^{-1} and (f) 2.5 mol L^{-1}.

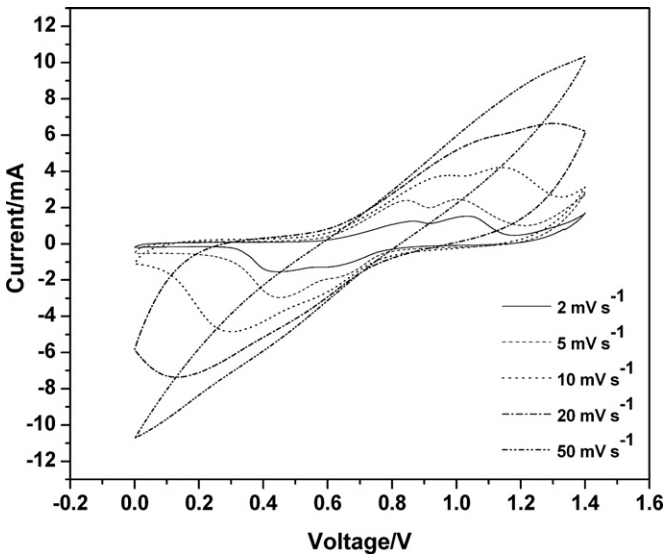

Fig. 5. CV curves of the $Li_4Mn_5O_{12}$ electrode at different scan rates in 1 mol L^{-1} Li_2SO_4.

curve according to the following equation [24,25]:

$$C = \frac{q_a + |q_c|}{2w\,\Delta V} \quad (1)$$

where $(q_a + |q_c|)$ is the sum of anodic and cathodic voltammetric charges on positive and negative sweeps, w is the mass of active material and ΔV is the potential window of CV. Based on Eq. (1), the single electrode discharge specific capacitance is 375 F g^{-1} at a scan rate of 5 mV s^{-1}, the value is nearly 1.5 times higher than that of obtained by sol–gel method [17]. The reason attributed to its higher capacitance is that the product is a porous spherical aggregation which has larger specific surface; its porous structure leads to sufficient electrolyte contact with active material, and increases the effective availability of active material, resulting in a good performance. With decreasing of the scan rate, discharge specific capacitance of the single electrode increased gradually.

Electrochemical impedance analysis

Impedance spectroscopy technique was applied to monitor resistance changes in electrolyte/$Li_4Mn_5O_{12}$ interface and the plots contain two parts of high and low frequency regions. The high frequency intercept of the semicircle with the real axis gives the internal resistance, including the resistance of the electrolyte, the intrinsic resistance of the active material, and the contact resistance at the interface active material/current collector. The internal resistance of the samples treated by different concentrations $(NH_4)_2S_2O_8$ are almost the same. The semicircle in the high frequency region suggests that there is a charge transfer resistance (*Rct*). As shown in Fig. 6, the semicircle radius of sample treated by 1.5 mol L^{-1} $(NH_4)_2S_2O_8$ is smaller than others, indicated that the sample has the smallest *Rct* and good electrochemical performance. The straight line in the low frequency region should be ascribed to the diffusion of Li^+ ions in $Li_4Mn_5O_{12}$ matrix. The lower impedance and better ionic diffusion leads to a good performance. The result is consistent with CV, hence, the sample used in the following test is the one that treated by 1.5 mol L^{-1} $(NH_4)_2S_2O_8$.

Charge/discharge test at a constant current density

The charge/discharge curves of $Li_4Mn_5O_{12}$/AC at a current density of 100 mA g^{-1} in 1 mol L^{-1} Li_2SO_4 are presented in Fig. 7. As shown, a good linear of potential vs. time is observed for all curves and the charge curves are symmetric to their corresponding discharge counterparts. The voltage drop is not observed

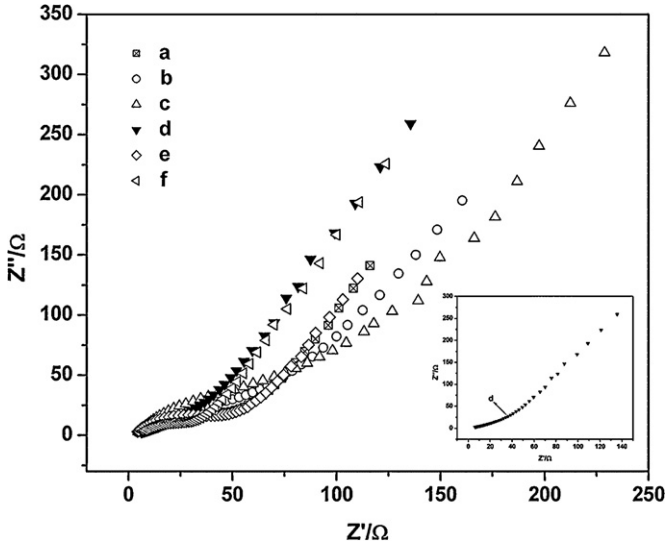

Fig. 6. Electrochemical impedance plots of $Li_4Mn_5O_{12}$ electrode with different concentration of $(NH_4)_2S_2O_8$ treatment. (a) 0.5 mol L^{-1}, (b) 0.7 mol L^{-1}, (c) 1.0 mol L^{-1}, (d) 1.5 mol L^{-1}, (e) 2.0 mol L^{-1} and (f) 2.5 mol L^{-1}.

when the current direction is changed, indicating that it is typical characteristic of an electrochemical capacitor. The mechanism of electrochemical reaction is expressed as follows. $Li_4Mn_5O_{12}$ takes advantage of Li^+ ions intercalate/extract to produce pseudocapacitance while AC adopts double layer capacitance. Under charge process, Li^+ ions extract from positive electrode, adhering on the AC surface. Under discharge process, Li^+ ions deadsorb from AC surface, then intercalate into positive electrode [26].

$$Li_{4+x}Mn_5O_{12} \underset{\text{discharge}}{\overset{\text{charge}}{\rightleftharpoons}} Li_4Mn_5O_{12} + xLi^+ + xe^- \quad (2)$$

$$AC + xLi^+ + xe^- \underset{\text{discharge}}{\overset{\text{charge}}{\rightleftharpoons}} AC(xe^-)//xLi^+(//\text{stands for double layer}) \quad (3)$$

Cycling ability test

Fig. 8 shows the cycling ability of $Li_4Mn_5O_{12}$ at a current density of 100 mA g^{-1} in 1 mol L^{-1} Li_2SO_4. With the increase of cycling times, the discharge specific capacitance begins to decrease from

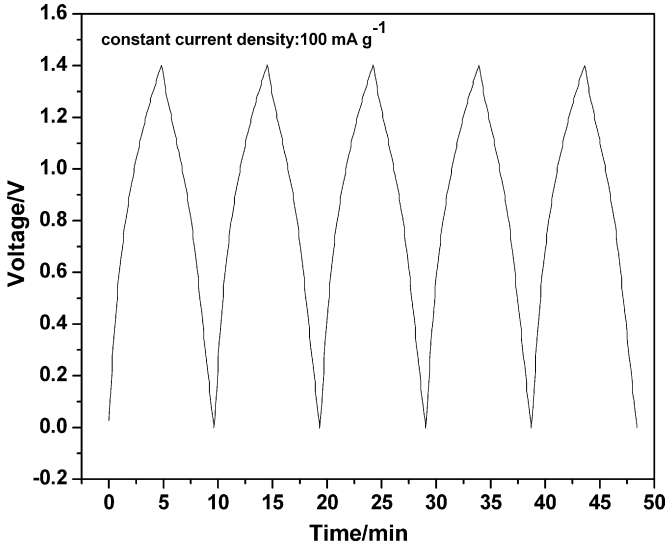

Fig. 7. Charge/discharge curves of the $Li_4Mn_5O_{12}$/AC asymmetric supercapacitor at a current density of 100 mA g^{-1} in 1 mol L^{-1} Li_2SO_4.

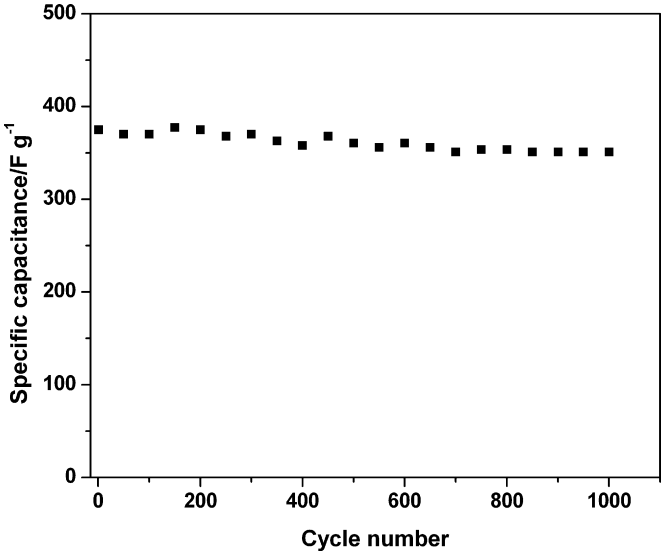

Fig. 8. Cycling ability of $Li_4Mn_5O_{12}$ at a current density of 100 mA g^{-1} in 1 mol L^{-1} Li_2SO_4.

375 to 351 F g^{-1} after 1000 cycles, and the value was cut down to less than 0.024 F g^{-1} per cycling period.

Conclusion

In this study, $Li_4Mn_5O_{12}$ porous spherical aggregation with a particle size of 3 μm was synthesized by hydrothermal method in which $LiMn_2O_4$ was used as precursor in the presence of oxidant $(NH_4)_2S_2O_8$. The concentration of $(NH_4)_2S_2O_8$ played a key role in the formation of porous spherical aggregation and the optimal concentration of oxidant was found to be 1.5 mol L^{-1}. The electrochemical test results showed that the porous spherical aggregation was able to deliver 375 F g^{-1} within potential range 0–1.4 V at a scan rate of 5 mV s^{-1} in 1 mol L^{-1} Li_2SO_4, and this value was cut down to less than 0.024 F g^{-1} per cycling period in 1000 cycles. The above results displayed that this electrode material exhibited a good performance.

Acknowledgements

This work was supported by the National Natural Science Foundation of China (No. 20701029). The authors gratefully thank the help of Xiaoyang Ji, Analytical and Testing Center at Sichuan University, for the XRD test.

References

[1] C. Bae, H. Yoo, S. Kim, K. Lee, J. Kim, M.M. Sung, H. Shin, Chem. Mater. 20 (2008) 756–767.
[2] N.R. Chiou, L.J. Lee, A.J. Epstein, Chem. Mater. 19 (2007) 3589–3591.
[3] T. Zhang, Q. Chen, L.M. Peng, Adv. Funct. Mater. 18 (2008) 3018–3025.
[4] Y.G. Li, B. Tan, Y.Y. Wu, Nano Lett. 8 (2008) 265–270.
[5] J.Y. Luo, H.M. Xiong, Y.Y. Xia, J. Phys. Chem. C 112 (2008) 12051–12057.
[6] Y. Wang, H. Yang, J. Am. Chem. Soc. 127 (2005) 5316–5317.
[7] L.X. Yang, Y.J. Zhu, W.W. Wang, H. Tong, M.L. Ruan, J. Phys. Chem. B 110 (2006) 6609–6614.
[8] Y. Zhang, R.Y. Li, X.R. Zhou, M. Cai, X.L. Sun, J. Phys. Chem. C 112 (2008) 10038–10042.
[9] D.H. Park, S.T. Lim, S.J. Hwang, C.S. Yoon, Y.K. Sun, J.H. Choy, Adv. Mater. 17 (2005) 2834–2837.
[10] Y.N. Xia, P.D. Yang, Y.G. Sun, Y.Y. Wu, B. Mayers, B. Gates, Y.D. Yin, F. Kim, H.Q. Yan, Adv. Mater. 15 (2003) 353–389.
[11] C. Pacholski, A. Kornowski, H. Weller, Angew. Chem. Int. Ed. 41 (2002) 1188–1191.
[12] Q.G. Li, J.B. Olson, R.M. Penner, Chem. Mater. 16 (2004) 3402–3405.
[13] Y. Tian, D.R. Chen, X.L. Jiao, Y.Z. Duan, Chem. Commun. (2007) 2072–2074.
[14] Y. Tanaka, Q.W. Zhang, F. Saito, Powder Technol. 132 (2003) 74–80.

[15] D.K. Kim, P. Muralidharan, H.W. Lee, R. Ruffo, Y. Yang, C.K. Chan, H. Peng, R.A. Huggins, Y. Cui, Nano Lett. 8 (2008) 3948–3952.
[16] X.X. Li, F.Y. Cheng, B. Guo, J. Chen, J. Phys. Chem. B 109 (2005) 14017–14024.
[17] Y.G. Sun, Y.N. Xia, Science 298 (2002) 2176–2179.
[18] Y.J. Hao, Y.Y. Wang, Q.Y. Lai, Y. Zhao, L.M. Chen, X.Y. Ji, J. Solid State Electrochem. 13 (2009) 905–912.
[19] H.Y. Chu, Q.Y. Lai, Y.J. Hao, Y. Zhao, X.Y. Xu, J. Appl. Electrochem. 39 (2009) 2007–2013.
[20] B.J. Huang, R. Santhanam, D.G. Liu, J. Power Sources 101 (2001) 86–89.
[21] Joint Committee on Power Diffraction Standards, card no. 14-0117.
[22] R.L. Penn, J.F. Banfield, Science 281 (1998) 969–971.
[23] L.P. Xu, Y.S. Ding, C.H. Chen, L.L. Zhao, Chem. Mater. 20 (2008) 308–316.
[24] C.C. Hu, C.C. Wang, Electrochem. Commun. 4 (2002) 554–559.
[25] X.Y. Wang, X.Y. Wang, W.G. Huang, P.J. Sebastian, S. Gamboa, J. Power Sources 140 (2005) 211–215.
[26] Y. Zhao, X.Y. Xu, Q.Y. Lai, Y.J. Hao, L. Wang, Z.E. Lin, J. Solid State Electrochem. (2009) doi:10.1007/s10008-009-0970-7.